Excess Polarizability Reveals Exciton Localization/Delocalization Controlled by Linking Positions on Porphyrin Rings in Butadiyne-Bridged Porphyrin Dimers

Chunxing She,[†] Shanmugam Easwaramoorthi,[‡] Pyosang Kim,[‡] Satoru Hiroto,[§] Ichiro Hisaki,[§] Hiroshi Shinokubo,[§] Atsuhiro Osuka,*[,§] Dongho Kim,*[,‡] and Joseph T. Hupp*[,†]

Department of Chemistry, Northwestern University, 2145 Sheridan Road, Evanston, Illinois 60208, Spectroscopy Laboratory for Functional π-Electronic Systems and Department of Chemistry, Yonsei University, Seoul 120-749, Korea, and Department of Chemistry, Graduate School of Science, Kyoto University, Kyoto 606-8502, Japan

Received: September 10, 2009; Revised Manuscript Received: February 11, 2010

We report direct measurements of the excess polarizability volumes of butadiyne-bridged zinc porphyrin dimers at singly β-to-β (**1Zn**) and doubly β-to-β (**2Zn**) positions using the transient dc photoconductivity (TDCP) technique. The excess polarizability volumes of the singlet exciton for **1Zn** and **2Zn** are 110 and 270 Å^3, respectively, while those of the triplet exciton are ∼100 Å^3 for both dimers. Our measurements suggest that the singlet exciton is mainly localized on one porphyrin subunit for **1Zn**, similar to the case for the porphyrin monomer. While the exciton is fully delocalized on two porphyrin subunits in the case of meso-to-meso linked dimer (**3Zn**), the extent of exciton localization/delocalization for doubly β-to-β linked dimer lies between those of singly β-to-β and meso-to-meso linked dimers. Electronic structure calculations show that the dramatically different extents of exciton localization/delocalization are the results of frontier orbital coefficients being small at β positions but large at meso positions. Two butadiyne linkages between the porphyrins at β positions (**2Zn**) clearly facilitate electronic communication between the two porphyrin subunits by virtue of stabilization of cumulenic charge resonance structures through enforced planarity.

Introduction

Conjugated porphyrin oligomers have been the subject of intense interest due to their unique optical and electronic properties for the applications in cellular imaging,[1,2] charge transport in molecular wires,[3,4] and searching for materials with possible two photon absorption (TPA) property.[5−10] These unique properties are the results of strong excitonic coupling and electronic communication among porphyrin subunits.[11−13] Two types of linkages have been employed, ethyne- and butadiyne-bridges, to connect porphyrin monomers through meso-to-meso, meso-to-β, or β-to-β positions. On the basis of red-shifted absorption maxima and frontier molecular orbitals of zinc porphyrin dimers, it is generally known that π-conjugation follows the order meso-to-meso > meso-to-β > β-to-β.[12,13] Among such covalently linked porphyrin dimers, meso-to-meso linked dimers are well understood to be highly conjugated molecular systems with singlet excitons fully delocalized on the two porphyrin subunits as well as bridges, as indicated by optical properties,[11−13] electronic structure calculations,[11,14−16] excess polarizability measurements,[17,18] and TPA measurements.[5−7,9,10] While TPA cross sections of meso-to-meso linked dimers have been well-studied and also suggested to have significant contributions due to one-photon processes,[9] conjugated β-to-β linked porphyrin dimers are less well-studied even though they evince enhanced TPA cross-section values.[19]

Previously, we reported the synthesis of a doubly β-to-β 1,3-butadiyne-bridged porphyrin dimer **2Zn** that shows enhanced TPA cross-section values as a result of a higher extent of π-conjugation compared to that for its singly β-to-β linked analogue **1Zn** (Chart 1).[19] While it is well conceived that planar structures ensure π-conjugation,[19] the linking positions on porphyrin rings also play a major role in determining the extent of π-conjugation.[13,20] Although strong excitonic coupling is directly reflected in the absorption spectra, a direct measurement of excess polarizability volumes that depend on the size of excitons is crucial for understanding quantitatively the strength of excitonic coupling among multiple porphyrin subunits and the dramatic enhancement of TPA cross-section values for this type of porphyrin oligomer.[5,6]

CHART 1: Structures of Porphyrin Dimers Linked through Different Positions

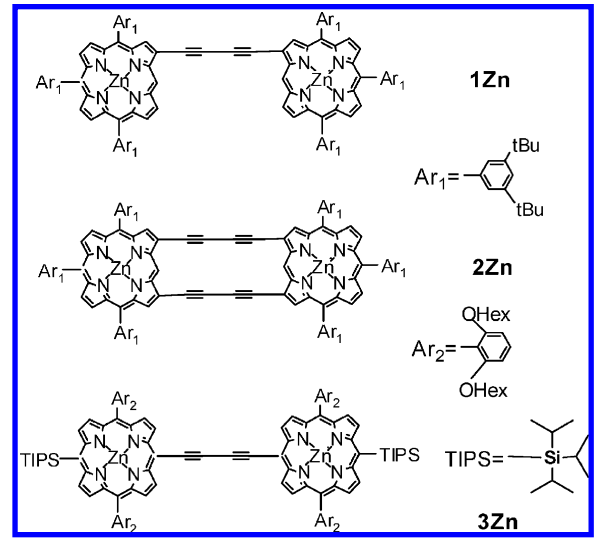

* Corresponding authors. E-mails: A.O., osuka@kuchem.kyoto-u.ac.jp; D.K., dongho@yonsei.ac.kr; J.T.H., j-hupp@northwestern.edu.
† Northwestern University.
‡ Yonsei University.
§ Kyoto University.

10.1021/jp908767x

TABLE 1: Intersystem Crossing Yields (ϕ_{isc}) and Times (τ_{isc}), Observed Fluorescence Quantum Yields (ϕ_f) and Lifetimes (τ_0), Excited-State Lifetimes without Intersystem Crossings (τ_F), $S_1 \rightarrow S_0$ Internal Conversion Time (τ_{ic}) and Q-Band Absorption Maximum (λ^Q_{max}) for 1Zn, 2Zn, and 3Zn

compound	ϕ_{isc}	τ_{isc} (ns)	ϕ_f	τ_F (ns)	τ_{ic} (ns)	τ_0 (ns)	λ^Q_{max} (nm)
1Zn	0.67 ± 0.07^b	3.0 ± 0.3^b	0.12^a	6.1 ± 1.2^b	9 ± 3^b	1.97^a	606^a
2Zn	0.65 ± 0.06^b	2.7 ± 0.3^b	0.009^a	5.3 ± 0.9^b	5.4 ± 0.1^b	1.78^a	645^a
3Zn[c]	0.46	2.8	0.20	2.4	3.8	1.3	715

[a] Date taken from ref 19. [b] The values were obtained by fitting τ_{isc} and τ_{ic} so that k_{ic} increases with λ^Q_{max} based on the energy gap law[28] for ten porphyrin monomer and oligomers, five of which are published in ref 18. [c] Data taken from ref 18 for comparison to justify values of τ_{ic} for **1Zn** and **2Zn**.

In this work we measured directly the excess polarizability volumes of butadiyne-bridged dimers linked at singly β-to-β (**1Zn**) and doubly β-to-β (**2Zn**) positions using the transient dc photoconductivity (TDCP) technique. The TDCP technique measures the photoinduced change of solute polarization caused by changes in both permanent and induced dipole moments in an applied field.[21−25] For symmetrical **1Zn** and **2Zn** lacking permanent dipole moments, the TDCP signals originate from the photoinduced excess molecular polarizability ($\Delta\alpha$), which leads to the field-induced dipole moments, $\Delta\mu^*$ ($\Delta\mu^* = E \times \Delta\alpha$, where E is the applied electric field).[18,26] The excess polarizability volumes, $\Delta\alpha_V$ ($\Delta\alpha_V = \Delta\alpha/4\pi\varepsilon_0$, where ε_0 is the vacuum permittivity) of singly and doubly β-to-β linked dimers are compared with those of porphyrin monomer (**ZnP**) and another butadiyne-bridged dimer linked at meso-to-meso positions, **3Zn** (Chart 1).[17,18] By correlating the excess polarizability volumes with the extent of exciton localization/delocalization, we observed that both the singlet and triplet excitons are mainly localized on one porphyrin subunit for **1Zn** and are similar to that of **ZnP**,[17,18] confirming what has been observed for a similar porphyrin dimer in EPR measurements.[27] While the singlet exciton is fully delocalized on the two porphyrin subunits in the case of **3Zn**,[18] the extent of exciton localization/delocalization for **2Zn** lies between those of **1Zn** and **3Zn**. Electronic structure calculations show that the dramatically different extents of exciton localization/delocalization are the results of frontier orbital coefficients being small at β positions but large at meso-positions. Double linkages (as opposed to single linkage) through β positions in **2Zn** clearly facilitate electronic communication between two porphyrin subunits.

Experimental Section

Synthesis of butadiyne-bridged porphyrin dimers was reported previously.[18,19] 1,4-Diazabicyclo[2.2.2]octane (DABCO), $CHCl_3$ and toluene (HPLC grade) were purchased from Aldrich without further purification. Absorption spectra were collected using a CARY 5000 UV−vis−NIR spectrophotometer. Other photophysical measurements except the intersystem crossing yields (which were estimated on the basis of the energy gap law;[28] see Table 1) have been reported in previous publications.[18,19]

TDCP Measurements. All measurements were performed with instrumentation described previously.[18,22−25,29] Briefly, a 1000 V potential was applied across a 0.25 mm gap between two electrodes. The samples were excited at 470 nm (10 Hz, ~2 ns fwhm) with an Opotek Vibrant OPO laser pumped with the third harmonic of a Quantel Brilliant Nd:YAG laser. Solutions were purged with N_2 for 15−20 min before excitation.

TDCP Analysis. The methodology of TDCP data analysis has been fully detailed elsewhere.[18,29] The displacement current, dQ/dt (where Q is charge), which is monitored by a digital scope (input impedance $R = 50\ \Omega$), gives rise to a transient voltage, $v(t)$, that can be described by the following equation:

$$v(t) + \tau_{RC}\frac{dv(t)}{dt} = RS\frac{dP}{dt} \propto \frac{dn_e}{dt} \quad (1)$$

where P is the polarization of solute (in nonpolar solvents). The photoinduced change in P is proportional to the change in excited-state population n_e. τ_{RC} is the RC time constant. S is the surface area of the parallel measuring plates in the capacitance cell. In the case of a three-state-model with ground state (G), singlet excited state (S), and triplet excited state (T) (see Scheme 1), the following solution was used (simplified from equation S1 in ref 18 using the condition $\tau_T \gg \tau_{isc}$) to dissect the signal contributions from the singlet ($^1\Delta\alpha_V$) and triplet ($^3\Delta\alpha_V$) polarizabilities.

$$v(t) = H\frac{d}{dt}\{{}^3\Delta\alpha \times e^{-t/\tau_T} - {}^1\Delta\alpha \times e^{-t/\tau_r} + e^{-t/\tau_{isc}} \times ({}^1\Delta\alpha - {}^3\Delta\alpha)\} \quad (2)$$

where H is a constant experimental factor detailing the contributions of solvent and E in the experiment. τ_r is the time constant for chromophore rotation.

SCHEME 1: Three-State Model with Ground State (G), Singlet Excited State (S), and Triplet Excited State (T)[a]

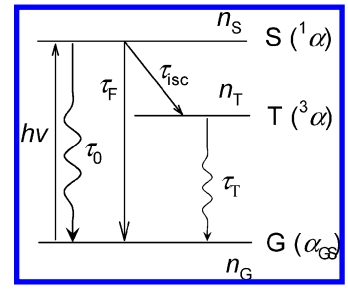

[a] $\tau_0 = 1/(k_f + k_{ic} + k_{isc})$, $\tau_F = 1/(k_f + k_{ic})$, $\tau_{isc} = 1/k_{isc}$, $\tau_T \gg 1\ \mu s$. $^3\Delta\alpha_V = {}^3\alpha - \alpha_{GS}$, and $^1\Delta\alpha_V = {}^1\alpha - \alpha_{GS}$.

Electronic Structure Calculations. Molecular geometries were optimized using Gaussian 03 at the B3LYP/6-31G* level.[30] The geometry-optimized structure at the same level of theory was used as an input for TD-DFT calculations.

Semiempirical Calculations. Molecular geometries were optimized at the AM1 level and then single point ZINDO-1 calculations were performed using HyperChem Pro 6.0. The molecular volume (V) and molecular polarizability of the ground state (α_{GS}) were then calculated using the QSAR package in HyperChem Pro 6.0.

Results and Discussion

π-Conjugation Indicated by Ground-State Absorption. Figure 1 shows the ground-state absorption spectra of (a) **1Zn**, (b) **2Zn**, and (c) **3Zn**, measured in $CHCl_3$. The calculated

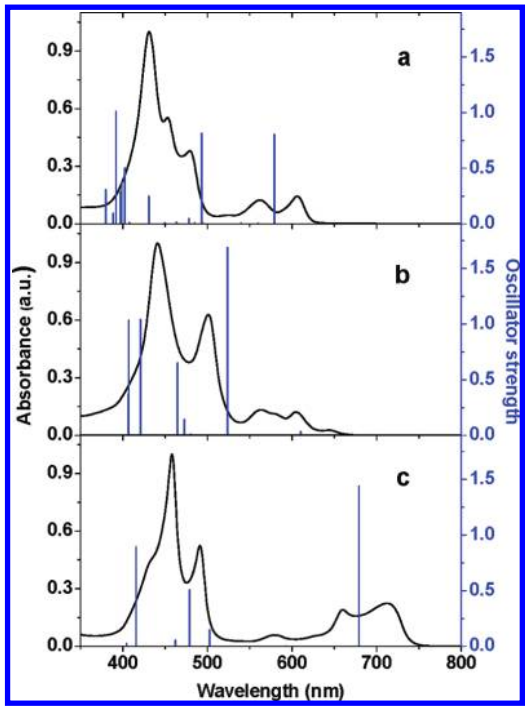

Figure 1. Absorption spectra of (a) **1Zn**, (b) **2Zn**, and (c) **3Zn** dissolved in $CHCl_3$. *Y* axes on the left and right sides correspond to the absorption spectra (black curves) and the stick spectra (blue lines), respectively.

oscillator strengths by using Gaussian 03 at B3LYP/6-31G* level for the three dimers are also shown for comparison. While both **2Zn** and **3Zn** show the strongest B bands at 441 and 460 nm, and red-shifted B bands at 501 and 493 nm, respectively, **1Zn** shows a B band at 452 nm together with additional bands at 431 and 479 nm, reflecting less degeneracy of transitions due to lower molecular symmetry compared with those of the other two molecules. Among these dimers, two porphyrin units are rigidly held by two butadiyne bridges for **2Zn**, wherein the contribution of conformational heterogeneity to the absorption spectra is quite unlikely. On the other hand, in **1Zn** and **3Zn** the single butadiyne allows free rotation around the bridge, and in principle a distribution of dihedral angles between the two porphyrin subunits is possible, as suggested by Therien et al. using semiempirical calculations for a similar compound.[13] Indeed, on the basis of temperature-dependent spectral data and computational methods, Anderson and Albinsson et al. suggested that meso−meso butadiyne-linked porphyrin dimers in the ground state are free to sample all the dihedral angles between 0° and 90° with little energy barrier.[31] Consequently, the blue-side B band for **3Zn** has been assigned to the $S_0 \rightarrow S_2$ transition for the twisted conformer while the red-side B band originates from the $S_0 \rightarrow S_2$ transition of the planar conformer along the butadiyne bridge.[31] For **1Zn**, the feasibility of conformational heterogeneity has been demonstrated by the formation of a supramolecular ladder aided by the binding of a bidentate ligand, 1,4-diazabicyclo[2.2.2]octane (DABCO) wherein (a) the possible rotation of porphyrin subunits around the butadiyne bridge is restricted and (b) a significant enhancement in the molecular coplanarity is obtained. Compared with that of **1Zn**, the UV−visible absorption spectrum of **1Zn** in ladder form (2:2 **1Zn:DABCO** complex; see the Supporting Information for the UV−visible titration spectra for the formation and disassociation of ladders, Figure S1−S3) shows a notable decrease in the intensity of B band at 452 nm (transition for nonplanar species) with a concomitant increase of intensity at 479 nm (transition for planar species). In fact, the UV−visible absorption spectra of **1Zn** and **2Zn** ladders in the B band region are remarkably similar in the way that the reddest B band is enhanced (due to planarization of two porphyrin subunits) apart from the relatively broader absorption peak of the **2Zn** ladder. This feature strongly suggests that a distribution of conformers of **1Zn** is present in the solution phase, but that the population of conformers with dihedral angles close to the planar is dominant. This suggestion is supported by the geometry optimization that the planar conformer is energetically more stable (vide infra) than its perpendicular conformer, consistent with what has been indicated for a similar porphyrin dimer.[13]

The Q absorption bands of **1Zn** and **2Zn** at ∼570 and 605 nm are similar. However, **2Zn** shows an extra weak Q-band at 645 nm, indicating more effective π-conjugation than **1Zn**. Electronic structure calculations predict that this extra Q-band has a relatively small oscillator strength (Figure 1b and Table S1, Supporting Information). The calculated oscillator strength for the HOMO → LUMO transition was found to be larger for **1Zn** (ca. 0.80) than **2Zn** (ca. 0.00; see Table S1 for more details). This unusually large oscillator strength for the HOMO → LUMO transition of **1Zn** is attributed to the relaxed selection rules due to reduced molecular symmetry as well as to possible rotation around the butadiyne bridge.

The Q absorption peaks of **1Zn** and **2Zn** are dramatically different from those of **3Zn**. **3Zn** has a strongly allowed transition along the butadiyne bridge linked through meso-positions; thus the Q-band is further red-shifted (715 nm). The larger oscillator strength (or intensity) of the Q-band than the B band is attributed to the strong electronic interaction between the two porphyrin subunits that splits Gouterman's four orbitals of monomer into at least eight frontier orbitals,[16,31] consistent with the findings of strong electronic and exitonic couplings made earlier for similar dimers.[13] This eight-orbital model qualitatively describes the absorption spectrum, predicting that the lowest transition (Q-band) becomes quasi-forbidden by configuration interaction. Collectively, the comparison of Q absorption bands points out the effectiveness of π-conjugation in the order **3Zn** > **2Zn** > **1Zn**.

Exciton Localization/Delocalization Probed by TDCP. To interpret TDCP responses of **1Zn** and **2Zn**, three photophysical data are needed, that is, singlet-to-triplet intersystem crossing rates ($\tau_{isc} = 1/k_{isc}$), singlet excited-state lifetimes without intersystem crossings ($\tau_F = 1/(k_f + k_{ic})$), and triplet excited-state lifetimes (τ_T). Typically, τ_T (≫1 μs) is much longer than the pulse duration (∼2 ns) for this type of porphyrin oligomer,[15,32] and thus its precise value is not required in the data analysis (see eq 2). Table 1 summarizes all the photophysical data (i.e., observed fluorescence lifetimes ($\tau_0 = 1/(k_f + k_{ic} + k_{isc})$) and fluorescence quantum yields (ϕ_f), intersystem crossing yields (ϕ_{isc}), $S_1 \rightarrow S_0$ internal conversion time ($\tau_{ic} = 1/k_{ic}$), τ_{isc}, τ_F, and Q-band absorption maximum (λ^Q_{max})) that were used in data analysis. The photophysical data for **3Zn** are taken from ref 18 for comparison.

Figure 2 shows TDCP signals for **1Zn** and **2Zn** dissolved in toluene. From eqs 1 and 2, the shapes of signals (amplitude vs time) should represent the excited-state population change (dn_e/dt) versus time. For an excited state that is short-lived and comparable to the temporal width of the laser pulse, n_e is proportional to the instantaneous pulse intensity, and dn_e/dt resembles the first derivative of the laser pulse shape. **2Zn** approximately satisfies this condition and indeed displays a derivative-like signal. The positive peak originates from the creation of the more polarizable singlet excited state (compared

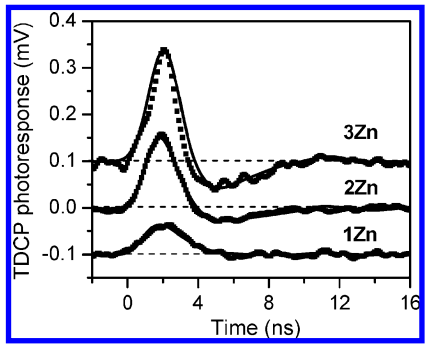

Figure 2. TDCP signals for **3Zn**, **2Zn**, and **1Zn** dissolved in toluene (dots, experimental data; solid lines, fits). The signals are scaled to correspond to the same absorbed energy and then vertically shifted so that the signal size reflects the relative polarizability changes.

TABLE 2: Photoinduced Polarizability Volume Changes of Singlet ($^1\Delta\alpha_V$) and Triplet ($^3\Delta\alpha_V$) Excited States for 1Zn, 2Zn, and 3Zn

compound	$^1\Delta\alpha_V$ (Å^3)[a]	$^3\Delta\alpha_V$ (Å^3)[a]	V (Å^3)[b]	α_{GS} (Å^3)[b]
1Zn	110 ± 20	90 ± 10	2900	130
2Zn	270 ± 40	100 ± 10	2800	140
3Zn[c]	430 ± 40	100 ± 50	3800	170

[a] Obtained from TDCP fitting. [b] Molecular volume (V) and molecular polarizability of the ground state (α_{GS}) were calculated using the QSAR package in HyperChem Pro 6.0. Molecular geometries were optimized at the AM1 level and then single point ZINDO-1 calculations were performed. [c] Data taken from ref 18.

to the ground state) and its preferential orientation in the applied electric field. The negative peak is a result of the decay of the more polarizable singlet excited state to a less polarizable state, e.g., ground state. When the singlet excited state quickly decays to another less-polarizable and long-lived state, such as the triplet excited state in **2Zn**, the negative-going peak will be attenuated so that the integrated area is smaller than that of the positive-going peak. An analysis of TDCP data shows that the excess polarizability volumes for the singlet ($^1\Delta\alpha_V$) and triplet ($^3\Delta\alpha_V$) states of **2Zn** are ∼270 and ∼100 Å^3, respectively.

A complete attenuation of the negative-going peak is expected when the singlet state is equally as polarizable as that of the long-lived triplet states, as in the case for **1Zn** (Figure 2). Indeed, an analysis of TDCP data for **1Zn** indicates that $^1\Delta\alpha_V$ (∼110 Å^3) and $^3\Delta\alpha_V$ (∼90 Å^3); these are identical within experimental errors and comparable to those of the porphyrin monomer.[17,18] (This complete attenuation can also be due to a short-lived singlet state, which almost fully decays to a long-lived triplet state, as shown for the porphyrin monomer[18] and Pt(II) diimine complexes.[26]) $^1\Delta\alpha_V$, $^3\Delta\alpha_V$, calculated molecular volumes (V), and ground-state molecular polarizabilities (α_{GS}) are summarized in Table 2.

The different excess polarizability volumes indicate different exciton localization/delocalization in porphyrin dimers studied here. As has been shown by Therien et al.[27] through EPR measurements, and by Warman et al.[17,33] and Hupp et al.[18] through the measurements of molecular polarizability, the singlet exciton for meso-to-meso linked conjugated porphyrin dimers is delocalized extensively on the two porphyrin subunits while the triplet exciton is largely localized on just one porphyrin subunit. For **1Zn**, the observed equal singlet and triplet polarizability suggests that both the singlet and triplet excitons are mainly localized on one porphyrin subunit, consistent with the conclusion reached by Therien et al.[27] and similar to those of the monomer.[17,18] As for the doubly β-to-β linked dimer, the extent of localization/delocalization for the singlet exciton lies between those of singly β-to-β and meso-to-meso linked dimers, while the triplet exciton is localized on one porphyrin subunit. The extent of exciton localization/delocalization for the dimers studied here is also consistent with the relative shifts of their Q-band absorption maxima (see Table 1).

The ground-state molecular polarizabilities (α_{GS}) for **1Zn** and **2Zn** are nearly identical, indicating very similar ground-state electronic communication between the two porphyrin subunits in the two cases. This observation is further confirmed by molecular orbital calculations (vide infra) showing that the HOMOs of the two compounds feature similar frontier orbital coefficients over the two porphyrin subunits and connecting bridge. From perturbation theory, the ground-state polarizability depends on both the transition dipole moments $\langle M_{fi}\rangle$ (i and f denote the ground and first-excited states, respectively) and the energy differences (ΔE_{fi}) between the ground and first-excited states

$$\alpha_{GS} \propto \sum \frac{|M_{fi}|^2}{\Delta E_{fi}} \qquad (3)$$

$\langle M_{fi}\rangle$ and ΔE_{fi} are expected to be similar for the two compounds on the basis of the similar extinction coefficients of Q-bands and the Q-band absorption peak maxima (or HOMO−LUMO gap, vide infra), respectively.[19] Thus α_{GS} values are identical for **1Zn** and **2Zn**, while it is expected to be slightly larger for **3Zn** on the basis of the red-shifted Q-band and its intensity (Table 2).

Frontier Molecular Orbitals. Electronic structure calculations were performed to provide further insight into the localization/delocalization of singlet excitons in the dimers studied here. Figure 3 shows the MO diagrams of **1Zn**, **2Zn**, and **3Zn** calculated using Gaussian 03 at B3LYP/6-31G* level.[30] The geometry optimized structures at the same level were used as inputs for TD-DFT calculations. The overall planarity of porphyrin subunits in all the dimers is conserved irrespective of bridging position, except for a small deviation in overall planarity for **1Zn** (see the Supporting Information). In addition, the bond length alternations of butadiyne bridges of **1Zn** and **2Zn** were calculated to be similar, further suggesting that the ground-state π-conjugation pathway is not significantly affected by the number of bridges. This observation is consistent with the identical α_{GS} values for **1Zn** and **2Zn**.

The molecular orbitals of **1Zn**, **2Zn**, with **3Zn** are compared to examine the influence of meso−meso and β−β linking positions on exciton localization/delocalization. The MO energy levels and frontier orbital coefficients are significantly perturbed by β and the meso butadiyne substituent. The MO energy levels of Zn porphyrin (**ZnP**) are also shown in Figure 3 as a reference. The most salient feature in the MOs of all the dimers, irrespective of the bridging position, is the bridging-group-localized electron density apparent in the HOMO and LUMO. Furthermore, all the LUMOs of **1Zn**, **2Zn**, and **3Zn** show the extensive cumulenic character, consistent with earlier reports.[11,12,14] The largest impact by the substituent is seen on **3Zn** in which the destabilization of the HOMO (a_{2u}) energy from porphyrin monomer was calculated to be 0.6 eV and also the degeneracy of the LUMO and LUMO+1 is broken due to unsymmetrical substitution at meso-positions. The larger splitting between the HOMO and HOMO+1, LUMO and LUMO+1 energy levels (ca. 0.46 eV) causes a reduction in the configuration interaction among the MOs, thereby leading to the red-shifted absorption

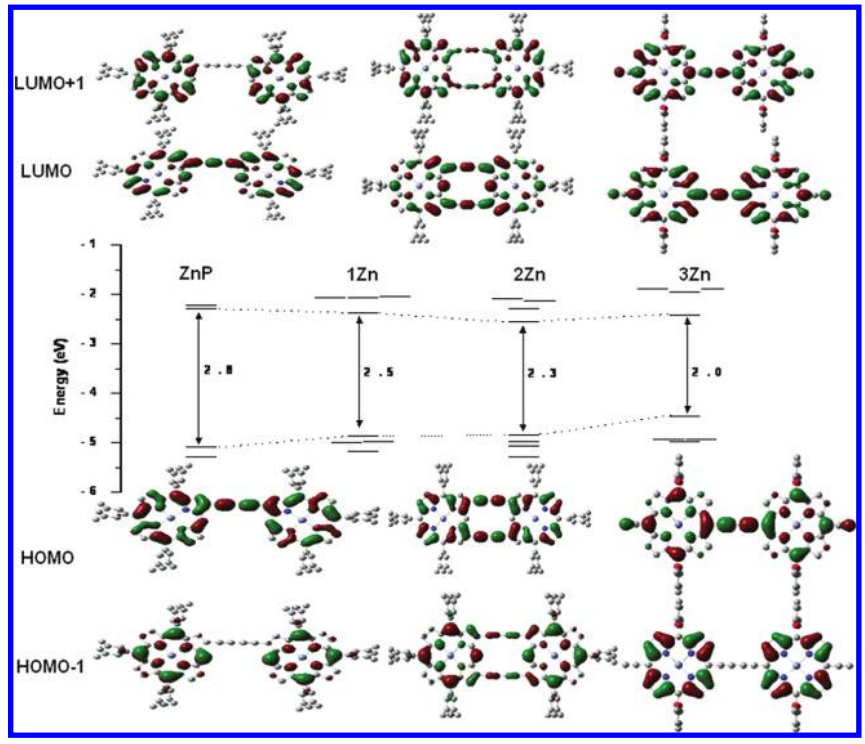

Figure 3. Frontier molecular orbitals (TD-DFT, B3LYP/6-31G*) and energy levels of optimized structures of **1Zn**, **2Zn**, and **3Zn**. The energy levels of ZnP are also shown for comparison.

spectra accompanied by changes in oscillator strengths. On the other hand, the destabilization of the HOMO of **1Zn** and **2Zn** relative to **ZnP** was calculated to be 0.22 and 0.25 eV, respectively. The comparatively smaller destabilization energy of the HOMO by the β-substituent delineates that the conjugation effect by the meso-substituent is larger than that of the β-substituent. The changes in the MO energy levels are very small when the number of bridges is increased from one (**1Zn**) to two (**2Zn**). Nevertheless, the electron density distribution for all the MOs is seemingly sensitive to the number of bridges, though the overall planarity of both **1Zn** and **2Zn** is essentially preserved. In particular, the HOMO (a_{1u}) of **2Zn** is symmetrically distributed over the two porphyrin subunits and butadiyne bridges. The HOMO of **1Zn** also shows a symmetrical electron density distribution over the two porphyrin subunits and the bridge; however, the a_{1u} type MO of the porphyrin subunit is slightly perturbed because of the unsymmetrical β-substitution. Thus the HOMO of **1Zn** possesses the a_{1u} character. While the HOMO−1 of **1Zn** (a_{2u}) has nodes at the β positions, that of **2Zn** exhibits notable electron density at the β and bridge positions. Despite the a_{2u} type MO of the porphyrin subunit in HOMO−1 for **2Zn**, the π-electron delocalization between porphyrin units through the butadiyne bridge is quite unique. Furthermore, despite the similar LUMOs for **1Zn** and **2Zn**, with notable electron density over the bridges having the cumulenic character, the LUMO+1 of **1Zn** possesses nodes at the butadiyne moiety but that of **2Zn** exhibits significant electron localization. Thus the HOMO−1 and LUMO+1 are quite different for **1Zn** and **2Zn**, and it is these MOs that play a crucial role in determining the conjugation efficiency.

The features of these molecular orbitals support the experimental excess polarizability measurements that the singlet exciton is fully delocalized on the two porphyrin subunits through the meso-bridge by means of the a_{2u} type HOMO. For β-substituted **1Zn** and **2Zn**, the localization of the exciton exclusively on one porphyrin subunit for the former as compared with the latter is attributable to the nodes at the β positions in the HOMO−1 and LUMO+1.

Two-Photon Absorption (TPA) Properties. From second-order perturbation theory,[34] the TPA cross-section values can be expressed as follows:[5,6]

$$\sigma_2^m = C \times \frac{|\mu_{i0}|^2 |\mu_{fi}|^2}{\left(\frac{\upsilon_{i0}}{\upsilon_{f0}} - \frac{1}{2}\right)^2 + \left(\frac{\Gamma_i}{2\upsilon_{f0}}\right)^2} \frac{1}{\Gamma_f} \tag{4}$$

where C is a constant taking into account the refractive index of medium and μ_{i0} and ν_{i0} are the $0 \rightarrow i$ transition dipole moment and frequency, respectively. Γ_f is the line width of the fth transition. $|\mu_{fi}|^2$ can be calculated using the excess molecular polarizability based on a four-state model:[5,6]

$$|\mu_{fi}|^2 = h\upsilon_{fi}\left(\frac{3}{2}\Delta\alpha + 2\frac{|\mu_{i0}|^2}{h\upsilon_{i0}} + \frac{|\mu_{k0}|^2}{h\upsilon_{k0}}\right) \tag{5}$$

Qualitatively, $|\mu_{fi}|^2$ increases with excess polarizability, $\Delta\alpha_V$.

The TPA cross-section value of **2Zn** (~9000 GM) was observed to be higher than that of **1Zn** (~5000 GM).[19] Similarly, it was shown that the TPA cross-section value of a β,β-2,5-thienylene bridged porphyrin dimer is doubled (from 3300 to 7200 GM at 800 nm) when the number of bridges between the porphyrin subunits is increased from one to two.[35] In both cases, the important aspect apart from the enforced molecular planarity by the double bridges could be the increased number of bridges that aids the global delocalization of π-electrons between the porphyrin subunits. The increase in TPA cross-section values can also be understood qualitatively in terms of the higher excess polarizability volume of **2Zn** (270 Å^3) than that of **1Zn** (110 Å^3). Equations

4 and 5 predict that the TPA cross-section values will increase with the excess molecular polarizability. This trend is also consistent with the effectiveness of π-conjugation in **2Zn** compared with **1Zn**. Furthermore, it was shown that strong electronic coupling between the adjacent porphyrin subunits by virtue of cumulenic resonance structure enhances both TPA cross-section values[6] and excess polaraizabilty.[17] On the other hand, for **1Zn** only the LUMO shows a cumulenic charge resonance structure, whereas the LUMO+1 possess nodes at the β position and the butadiyne bridge. Thus we can conclude that the nearly 2-fold increase in the excess polarizability and TPA cross-section value for **2Zn** with respect to **1Zn** arises from the increased π-electron delocalization between the two bridges and the stabilization of a cumulenic charge resonance structure by the enforced planarity of the molecule.

The TPA cross-section value of **3Zn** measured by the two-photon excited fluorescence method reported in ref 6 corresponds to 9100 GM for 873 nm photoexcitation. Though the TPA cross-section value for **2Zn** and **3Zn** are nearly equal, we do not compare these results as they were measured under different experimental conditions. However, it should be noted that the larger excess polarizability of **3Zn** despite a single bridge is due to the stronger electronic interaction through cumulenic charge resonance structures by meso-positions.

Conclusions

The excess polarizability volumes of the singlet excited states of singly linked and doubly linked dimers are 110 and 270 Å^3, respectively, while the excess polarizability volumes of the triplet excited states are about 100 Å^3. These results in conjunction with the MO calculations indicate that the number of linkers at the β position (due to difference in orbital coefficients) play a crucial role in the localization/delocalization of singlet excitons. Two butadiyne linkers at the β position lead to partial delocalization of singlet excitons on the porphyrin subunits. In addition, the stabilization of cumulenic charge resonance structure of the bridge by the enforced planarity of the doubly linked dimer enhances the TPA-cross section value and excess polarizability. Nonetheless, the larger excess polarizability for the meso−meso linked dimer (430 Å^3), despite only a single bridge, is due to the larger frontier orbital coefficients at the meso-position than at β ones. Our findings are consistent with the most red-shifted Q-band maximum observed only for meso-substituted porphyrins. Furthermore, the triplet exciton is confined to a single porphyrin subunit and is quite insensitive to the linking position[27] and the number of linkers.

Acknowledgment. C.S. and J.T.H. gratefully acknowledge the Weinberg College of Arts and Sciences, and the Basic Energy Sciences Program, Office of Science, U.S. Department of Energy, for financial support of our work (grant No. DE-FG02-87ER13808). The work at Yonsei was financially supported by the Star Faculty and World Class University (No. 2008-8-1955) programs of the Ministry of Education, Science, and Technology of Korea and a grant from the Fundamental R&D Program for Core Technology of Materials funded by the Ministry of Knowledge Economy, Republic of Korea. S.E. and P.K. are thankful for the BK21 fellowships. The quantum chemical calculations were performed by using the supercomputing resource of the Korea Institute of Science and Technology Information (KISTI). The work at Kyoto was supported by Grants-in-Aid for Scientific Research (No. 19205006 and 20108001 "pi-Space") from the Ministry of Education, Culture, Sports, Science, and Technology.

Supporting Information Available: Optimized geometries and details of electronic transitions for **1Zn**, **2Zn**, and **3Zn**. UV−visible spectrophotometric titration of **1Zn** and **2Zn**, respectively, with the bidentate ligand DABCO, indicating the formation and disassociation of ladder structures. This material is available free of charge via the Internet at http://pubs.acs.org.

References and Notes

(1) Kuimova, M. K.; Botchway, S. W.; Parker, A. W.; Balaz, M.; Collins, H. A.; Anderson, H. L.; Suhling, K.; Ogilby, P. R. *Nat. Chem.* **2009**, *1*, 69.
(2) Kuimova, M. K.; Collins, H. A.; Balaz, M.; Dahlstedt, E.; Levitt, J. A.; Sergent, N.; Suhling, K.; Drobizhev, M.; Makarov, N. S.; Rebane, A.; Anderson, H. L.; Phillips, D. *Org. Biomol. Chem.* **2009**, *7*, 889.
(3) Kocherzhenko, A. A.; Patwardhan, S.; Grozema, F. C.; Anderson, H. L.; Siebbeles, L. D. A. *J. Am. Chem. Soc.* **2009**, *131*, 5522.
(4) Grozema, F. C.; Houarner-Rassin, C.; Prins, P.; Siebbeles, L. D. A.; Anderson, H. L. *J. Am. Chem. Soc.* **2007**, *129*, 13370.
(5) Drobizhev, M.; Stepanenko, Y.; Dzenis, Y.; Karotki, A.; Rebane, A.; Taylor, P. N.; Anderson, H. L. *J. Am. Chem. Soc.* **2004**, *126*, 15352.
(6) Drobizhev, M.; Stepanenko, Y.; Dzenis, Y.; Karotki, A.; Rebane, A.; Taylor, P. N.; Anderson, H. L. *J. Phys. Chem. B* **2005**, *109*, 7223.
(7) Drobizhev, M.; Stepanenko, Y.; Rebane, A.; Wilson, C. J.; Screen, T. E. O.; Anderson, H. L. *J. Am. Chem. Soc.* **2006**, *128*, 12432.
(8) Easwaramoorthi, S.; Jang, S. Y.; Yoon, Z. S.; Lim, J. M.; Lee, C. W.; Mai, C. L.; Liu, Y. C.; Yeh, C. Y.; Vura-Weis, J.; Wasielewski, M. R.; Kim, D. *J. Phys. Chem. A* **2008**, *112*, 6563.
(9) Fisher, J. A. N.; Susumu, K.; Therien, M. J.; Yodh, A. G. *J. Chem. Phys.* **2009**, *130*, 134506.
(10) Zhu, L. Y.; Yi, Y. P.; Shuai, Z. G.; Schmidt, K.; Zojer, E. *J. Phys. Chem. A* **2007**, *111*, 8509.
(11) Anderson, H. L. *Chem. Commun.* **1999**, 2323.
(12) Lin, V. S. Y.; Dimagno, S. G.; Therien, M. J. *Science* **1994**, *264*, 1105.
(13) Lin, V. S. Y.; Therien, M. J. *Chem.—Eur. J.* **1995**, *1*, 645.
(14) Beljonne, D.; OKeefe, G. E.; Hamer, P. J.; Friend, R. H.; Anderson, H. L.; Bredas, J. L. *J. Chem. Phys.* **1997**, *106*, 9439.
(15) Shediac, R.; Gray, M. H. B.; Uyeda, H. T.; Johnson, R. C.; Hupp, J. T.; Angiolillo, P. J.; Therien, M. J. *J. Am. Chem. Soc.* **2000**, *122*, 7017.
(16) Wilson, G. J.; Arnold, D. P. *J. Phys. Chem. A* **2005**, *109*, 6104.
(17) Piet, J. J.; Taylor, P. N.; Anderson, H. L.; Osuka, A.; Warman, J. M. *J. Am. Chem. Soc.* **2000**, *122*, 1749.
(18) She, C.; McGarrah, J. E.; Lee, S. J.; Goodman, J. L.; Nguyen, S. T.; Williams, J. A. G.; Hupp, J. T. *J. Phys. Chem. A* **2009**, *113*, 8182.
(19) Hisaki, I.; Hiroto, S.; Kim, K. S.; Noh, S. B.; Kim, D.; Shinokubo, H.; Osuka, A. *Angew. Chem., Int. Ed.* **2007**, *46*, 5125.
(20) Yang, S. I.; Seth, J.; Balasubramanian, T.; Kim, D.; Lindsey, J. S.; Holten, D.; Bocian, D. F. *J. Am. Chem. Soc.* **1999**, *121*, 4008.
(21) Smirnov, S. N.; Braun, C. L. *J. Phys. Chem.* **1994**, *98*, 1953.
(22) Smirnov, S. N.; Braun, C. L. *Rev. Sci. Instrum.* **1998**, *69*, 2875.
(23) Walters, K. A.; Kim, Y. J.; Hupp, J. T. *Inorg. Chem.* **2002**, *41*, 2909.
(24) Vanhelmont, F. W. M.; Johnson, R. C.; Hupp, J. T. *Inorg. Chem.* **2000**, *39*, 1814.
(25) Vanhelmont, F. W. M.; Hupp, J. T. *Inorg. Chem.* **2000**, *39*, 1817.
(26) She, C.; Rachford, A. A.; Wang, X.; Goeb, S.; El-Ballouli, A. O.; Castellano, F. N.; Hupp, J. T. *Phys. Chem. Chem. Phys.* **2009**, *11*, 8586.
(27) Angiolillo, P. J.; Lin, V. S. Y.; Vanderkooi, J. M.; Therien, M. J. *J. Am. Chem. Soc.* **1995**, *117*, 12514.
(28) Englman, R.; Jortner, J. *Mol. Phys.* **1970**, *18*, 145.
(29) Smirnov, S. N.; Braun, C. L. *Chem. Phys. Lett.* **1994**, *217*, 167.
(30) Frisch, M. J. T.; G. W.; Schlegel, H. B.; Scuseria, G. E.; Robb, M. A.; Cheeseman, J. R.; Montgomery, J. A., Jr.; Vreven, T.; Kudin, K. N.; Burant, J. C.; Millam, J. M.; Iyengar, S. S.; Tomasi, J.; Barone, V.; Mennucci, B.; Cossi, M.; Scalmani, G.; Rega, N.; Petersson, G. A.; Nakatsuji, H.; Hada, M.; Ehara, M.; Toyota, K.; Fukuda, R.; Hasegawa, J.; Ishida, M.; Nakajima, T.; Honda, Y.; Kitao, O.; Nakai, H.; Klene, M.; Li, X.; Knox, J. E.; Hratchian, H. P.; Cross, J. B.; Bakken, V.; Adamo, C.; Jaramillo, J.; Gomperts, R.; Stratmann, R. E.; Yazyev, O.; Austin, A. J.; Cammi, R.; Pomelli, C.; Ochterski, J. W.; Ayala, P. Y.; Morokuma, K.; Voth, G. A.; Salvador, P.; Dannenberg, J. J.; Zakrzewski, V. G.; Dapprich, S.; Daniels, A. D.; Strain, M. C.; Farkas, O.; Malick, D. K.; Rabuck, A. D.; Raghavachari, K.; Foresman, J. B.; Ortiz, J. V.; Cui, Q.; Baboul, A. G.; Clifford, S.; Cioslowski, J.; Stefanov, B. B.; Liu, G.; Liashenko, A.; Piskorz,

P.; Komaromi, I.; Martin, R. L.; Fox, D. J.; Keith, T.; Al-Laham, M. A.; Peng, C. Y.; Nanayakkara, A.; Challacombe, M.; Gill, P. M. W.; Johnson, B.; Chen, W.; Wong, M. W.; Gonzalez, C.; and Pople, J. A. *Gaussian 03*, Revision C.02; Gaussian, Inc.: Wallingford, CT, 2004.

(31) Winters, M. U.; Karnbratt, J.; Eng, M.; Wilson, C. J.; Anderson, H. L.; Albinsson, B. *J. Phys. Chem. C* **2007**, *111*, 7192.

(32) Kuimova, M. K.; Hoffmann, M.; Winters, M. U.; Eng, M.; Balaz, M.; Clark, I. P.; Collins, H. A.; Tavender, S. M.; Wilson, C. J.; Albinsson, B.; Anderson, H. L.; Parker, A. W.; Phillips, D. *Photochem. Photobiol. Sci.* **2007**, *6*, 675.

(33) Piet, J. J.; Taylor, P. N.; Wegewijs, B. R.; Anderson, H. L.; Osuka, A.; Warman, J. M. *J. Phys. Chem. B* **2001**, *105*, 97.

(34) Boyd, R. W. *Nonlinear Optics*, 2nd ed.: Academic Press: Amsterdam, 2003; Chapter 12.

(35) Song, J.; Jang, S. Y.; Yamaguchi, S.; Sankar, J.; Hiroto, S.; Aratani, N.; Shin, J. Y.; Easwaramoorthi, S.; Kim, K. S.; Kim, D.; Shinokubo, H.; Osuka, T. *Angew. Chem., Int. Ed.* **2008**, *47*, 6004.

JP908767X